A NOVEL MULTIFUNCTIONAL ADDITIVE MANUFACTURED LATTICE STRUCTURE DESIGN FOR THERMAL AND MECHANICAL IMPROVEMENT OF LIQUID ROCKET

A NOVEL MULTIFUNCTIONAL ADDITIVE MANUFACTURED LATTICE STRUCTURE DESIGN FOR THERMAL AND MECHANICAL IMPROVEMENT OF LIQUID ROCKET ENGINE INJECTOR FACE PLATES

SPACE PROPULSION 2024
GLASGOW, SCOTLAND | 20 – 23 MAY 2024

Matteo Crachi [(1)], Tomas Cruz [(2)], Maximilian Strixner [(3)], Alexander Bee [(4)], Romain Mabboux [(2)], Wolfgang Armbuster[(4)], Raffaella Sesana [(1)]

[(1)] Politecnico di Torino , Torino, Italy, Email: matteo.crachi@polito.it
[(2)] The Exploration Company SAS, Merignac, France, Email: tomas@exploration.space
[(3)] The Exploration Company GmbH, Planegg, Germany, Email: maxi@exploration.space
[(4)] German Aerospace Center - DLR, Lampoldshausen, Germany, Email: alexander.bee@dlr.de

KEYWORDS: liquid rocket engine, propulsion components, injector head, L-PBF additive manufacturing, Inocnel718, heat transfer, thermo-mechanical analysis, material characterization

ABSTRACT:

The demand for increasing the efficiency in liquid rocket engines has led to a revaluation of the traditional design and manufacturing processes. Liquid rocket engines play a pivotal role in aerospace propulsion, and the performance of their injector head plates is crucial for achieving structural and thermal stability of the thrust chamber assembly. Additive manufacturing, specifically lattice structures, has emerged as a promising solution to enhance the thermal exchange and mechanical properties of various high requirements space components. The present work provides an overview of the application of additive manufacture lattice structures to improve the performance of injector head face plates in liquid rocket engines. Results will be referred to Nyx Moon capsule main thrust chamber assembly propulsion system - developed by The Exploration Company – and tested at German Aerospace Centre - DLR - Lampoldshausen P8 test facility.

1. INTRODUCTION

The Exploration Company is dedicated to democratizing space exploration by making it affordable, accessible, and inclusive. They achieve this through the development of innovative spacecraft like Nyx, designed for reusability and in-orbit refuelling. Nyx serves a wide range of missions, from extended orbits around Earth to lunar landings, with future capabilities including docking, refuelling, and cargo transportation.

At the heart of The Exploration Company's mission is the delivery of payloads to low Earth orbit (LEO) and their safe return aboard Nyx Earth. This spacecraft offers services to payloads, such as power, thermal management, and communication, catering to both pressurized and unpressurized cargo needs. As the company progresses, Nyx Earth components will be reused to facilitate lunar missions, integrating with cryogenic propulsion systems fueled by bio-methane (CH4) and liquid oxygen (LOX).

Nyx Moon expands the company's reach by facilitating cargo missions between Earth and the moon's surface, as well as within the cislunar environment, including docking with lunar space stations. To enhance its capabilities, Nyx Moon will master in-orbit refuelling, utilizing cryogenic propellants stored in orbit or produced on the moon.

Central to this propulsion system is the Huracan-engine, a liquid rocket engine developed for reusability, simplicity, and low-cost manufacturing.

The collaboration with the German Aerospace Center Institute of Space Propulsion in Lampoldshausen ensures the continued advancement and testing of this crucial engine's subsystems, including the injection head.

1.1. L-PBF Additive Manufacturing for liquid rocket engines injector heads

Liquid rocket engine injector heads serve the technical purpose of mixing liquid fuel and liquid oxidizer in a purposeful way for the following injection and ignition within the combustion chamber to propel the overall vehicle. The concept is known, but a general challenge is to find the optimum shape that will assure thermal and mechanical performance as desired. Along with finding this optimum shape, the inherent challenge is to find reasonable manufacturing technology. The geometrical shape of liquid rocket engine injector heads possesses a high degree of complexity and inner structure without accessibility from the outside, which excludes many

manufacturing technologies if the component is desired to be manufactured in one piece. A novel technology capable of realizing these complex metallic shapes in "Additive Manufacturing" (industrial 3D printing), where components are manufactured layer-by-layer.

Additive Manufacturing (AM) is an emerging technology used for producing intricate metallic components in rocket propulsion. AM offers numerous advantages over traditional methods, including reduced schedules, lower lifecycle costs, and enhanced performance due to intricate internal features. Components like injectors, combustion chambers, and nozzles exploit AM's benefits, addressing long lead times and tight tolerances. Designers can streamline part counts and eliminate complex assembly operations like brazing or welding. AM, a layer-by-layer fabrication method, contrasts with machining and assembly. Various AM techniques, utilizing powder and wire feedstock, have evolved over the past decade for fabricating combustion device components. This categorization helps in understanding the diverse approaches to AM in propulsion applications. A chart illustrates various metal additive manufacturing processes, based on prior work by Gradl et al. in 2018 [1].

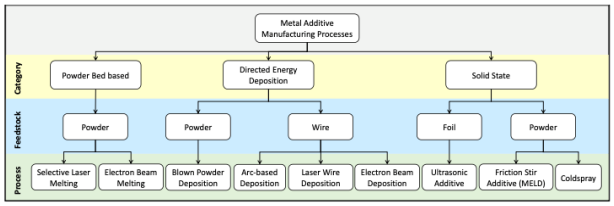

Figure 1: Overview of Metallic Additive Manufacturing Processes used in Component Development from Gradl et. Al, 2018 [1]

Due to the small feature sizes lattice structures, a fine process resolution is required. Considering all available processes for the desired material, the process of Laser Powder Bed Fusion (L-PBF, sometimes SLM: Selective Laser Melting) is capable of realizing the best and most suitable feature size resolution. With current state of the art, a general fine detail resolution of approximately 0.1mm can be achieved with L-PBF, which will be suitable for the demonstrated application. Another previous work by Gradl et.al in 2022 [2] shows the general achievable feature size resolution among AM process over the applicable deposition rate. The following figure demonstrates the suitability of L-PBF for the discussed application due to minimum achievable feature size. For the shown reasons, L-PBF was selected as the desirable manufacturing process for the application.

L-PBF utilizes a method, where the desired component features are fused layer by layer using a laser. In this project, L-PBF is applied to all components of combustion devices, including subassemblies like manifolds and flanges.

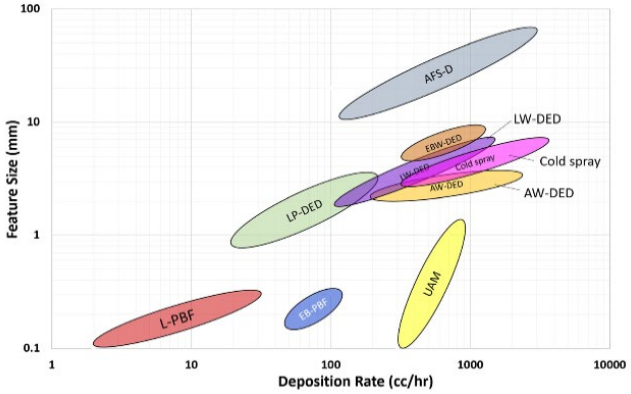

Figure 2: Feature size over deposition rate across AM processes from Gradl et. Al., 2022 [2]

The process begins with a 3D-CAD model sliced into thin 2D layers, guiding the laser's path for fusing the part. A fine-focus laser melts the metal powder, forming each layer according to the cross-section of the part. A build plate initiates bonding, and after each layer, it descends slightly for the next powder layer and laser fusion. Sufficient power ensures proper bonding between layers, allowing for intricate internal features such as coolant channels. The fabrication occurs in an inert environment to prevent oxidation. While L-PBF can produce complex parts, its scale is limited, with machines typically accommodating sizes up to 250mm x 250mm x 300mm (Gradl et. Al., 2018 [1]). Recent market developments however have shown larger scale systems capable of producing much larger parts. The following scheme illustrates the process of L-PBF with hardware components.

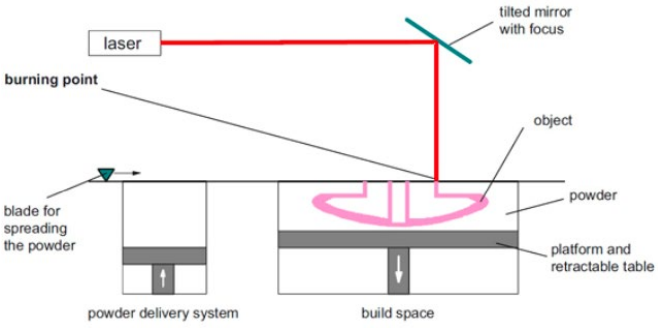

Figure 3: L-PBF process overview with hardware components

L-PBF production allows delicate steering of the energy source, in this case an assembly of high power fiber laser and scanner optics, to reach geometrical, thermal and mechanical performance. To achieve this, the melt pool is controlled in a way that is meaningful to create reasonable inner microstructure and surface quality. Therefore, laser parameters are commonly subdivided into in-fill and contour parameters. The following two figures illustrate such division into contouring and in-filling parameters in the L-PBF process.

Figure 4: Exposing with contour parameter from Gradl et. Al., 2018 [1]

Figure 5: Exposing with in-fill parameter from Gradl et. Al., 2018 [1]

A study from Bai et. al. in 2021 [3] proved, that lattice structures can significantly enhance performance in modern aerospace, water and land transportation and other mechanical fields. Especially functional gradient designs can open up new possibilities and solve technological problems. In the following figure, a mechanical study was conducted under the consideration of several different possible lattice geometries produced through L-PBF [3].

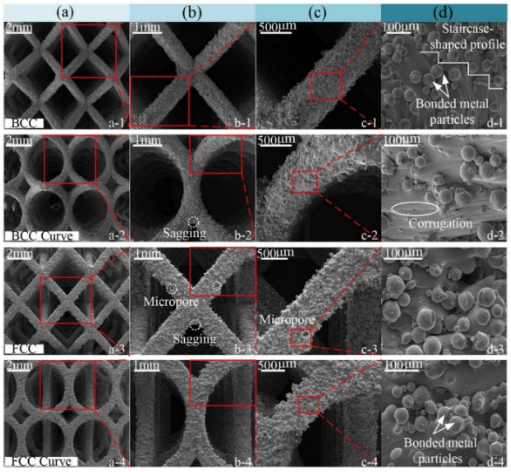

Figure 6: SEM micrography of different L-PBF lattice unit cells from Bai et. Al., 2021[3]

These considerations about the suitable manufacturing processes conclude, that:

- L-PBF is the best suitable process for the desired material and shape to realize
- Lattice structures through AM can significantly raise component performance for aerospace and thermal applications
- Feature size and resolution are still limited, but with good prospects of future progress

1.2. Liquid rocket engine injector head cooling strategies

Common strategies to cool down the face plate is to use a high conductive material for the face plate (e.g. copper and copper alloys), because of the high heat transfer properties of the material. This strategy could lead to multi-material and therefore high costs because of manufacturing and integration processes [5], [6].

Alternately, liquid rocket engines injector head face plate can be chilled by means of cooling channels inside the face plate.

High thrust liquid rocket engine can benefit from the high number of inject elements to reduce the face plate temperature (e.g. Vulcan engine [6]). Injects, because of the low temperature and high velocities of both propellants and oxidizers, tend to cool down the face plate. However, the number of injectors affects the design and the combustion stability. Therefore, It is not possible to freely increase the number of injectors because of the willingness to decrease the face plate temperature.

Nowadays porous injector head face plate [5], thanks to access to computational power, seem to be an alternative solution to the well know rigid mesh face plates [7][8][9]. This solution use a porous material for the injector head face plate, allowing a transpiration cooling mechanism.

1.3. Research question

This study presents an alternative design solution for liquid rocket engine injector head face plate, aiming to reduce temperature of the materials in contact with hot gases and improve the mechanical robustness of the hardware. The design consists of introducing functional lattice structure on the top of the injector head face plate.

2. MATERIAL AND METHODS

2.1. Water cooled TCA1 Huracan Test campaign

The first iteration of the Huracan Thrust Chamber Assembly (TCA1) has been successfully tested in 2023 at DLR Lampoldshausen test bench P8. For this first campaign, liquid oxygen and gaseous methane were fed to the Injector Head (IH) while water was substituting liquid methane as coolant.

The main objectives of the campaign are listed hereafter:

- Validate the hardware design and

manufacturing techniques used;
- Demonstrate reliable ignition and start-up transients;
- Demonstrate stable steady-state operation for a broad range of feeding conditions;
- Ensure proper combustion efficiency and stability;
- Provide data for models anchoring.

With a total of 12 hot fires for about 500s of steady-state operation, this campaign allowed to explore as low as 33% throttling, mixture ratios between 60% and 110% of the nominal point and various water coolant mass flows. In order to monitor the faceplate temperatures and the performance of the lattice structure, two thermocouples were placed between two swirl injectors of the two innermost rows. This location was chosen because it was expected to have the highest temperatures. In reality, the thermal loads to the faceplate are highly non-uniform and it is very common for hot spots to exist, which makes it unlikely that the thermocouples measure the actual hottest temperature. Therefore, the thermocouple data do not reflect the conditions on the entire faceplate but by choosing this region, we can have an estimate of the magnitude of the loads that we can expect. These two thermocouples have a distance of 4mm between each other in the plane of the faceplate. This distance comes from constraints in the assembly and can cause some errors due to the fact that the heat flux is not 1D. Additionally, one thermocouple was inserted at a depth of 0.5mm away from hot side of the faceplate, $T_{0.5mm}$, and the other one at 1mm, T_{1mm}. By implementing thermocouples at different depths, we can also get an estimate for the heat flux.

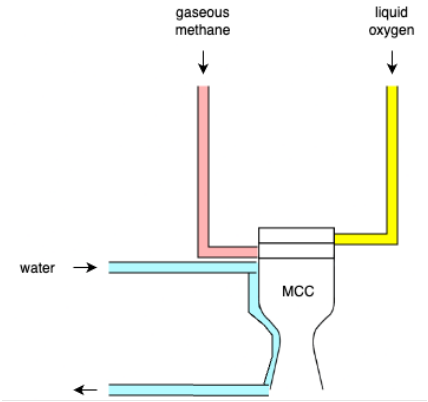

Figure 7: Huracan TCA1 testing layout

2.2. Generative algorithm

The design requirements for the lattice are to support the entire faceplate in order to prevent overhang surfaces and to improve heat transfer of the faceplate. In this section the generation of the lattice is discussed.

The creation of the lattice starts off by defining the domain that we want to fill with the lattice. Since we want to cover the entire faceplate with the lattice, one of the surfaces of this domain needs to be completely flat. However the only points of support for the lattice are the injectors and these naturally do not cover the entire surface of the faceplate. Therefore the most logical choice for the lattice domain is the union of discrete cones that start at the injector posts and grow outwards until they cover the faceplate. An elementary cone can be seen in Figure 8.The cones contain the inner volume of the injectors that is occupied by the fluid. This volume is removed at the end by a Boolean operation.

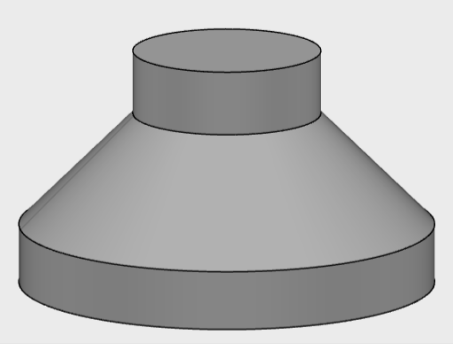

Figure 8: Elementary cone for the lattice domain

From the lattice domain we can compute a bounding box. This bounding box is subdivided by a unitary lattice cell. For this is it necessary to choose the lattice cell dimension, L, which is one of the main inputs for the design. That means that a cell is LxLxL. For this design, the lattice structure uses a body centred cubic crystalline structure, where each subsequent layer is shifted by $L/2$ in all directions.

Besides the lattice dimension, there are two other inputs for the design. These inputs are the beam diameter, d, and the beam length, l. The creation of the elementary cell starts with a cube with the side dimension L. The beams of the lattice are generated using the diagonals of this cube as the guide curves (see Figure 9). Note that the beam length is not necessarily equal to $\sqrt{3}L$, because in the region where all beams intersect there is a more voluminous region that strengthens the connection between beams. For this reason, it is sometimes convenient to describe the beam length as the a fraction of the length of the diagonal, $p = \frac{l}{\sqrt{3}L}$. In order to reduce weight, it is ideal to minimize the density of the lattice, meaning that the portion of the bounding box that is occupied by the lattice should be as small as possible. This can be achieved by reducing the beam diameter and increasing the beam length; however these two parameters have strong implications on the strength of the lattice and are usually constrained by the mechanical requirements.

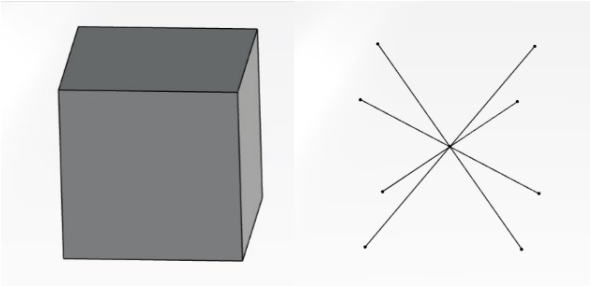

Figure 9: elementary cell cube on the left, skeletal lattice composed by the diagonals of the cube on the right

To generate the entire lattice, the elementary skeletal lattice element composed by the diagonals of the cube is used to tile the entire bounding box. Then all beams that are partially or fully outside the lattice domain are completely removed. This aspect is very important to prevent any partial beams to be generated which would create overhang surfaces. Since the removal of beams is very dependent on the location of the cell in the bounding box, there can be many different lattice cells depending on the number of beams, just as we see in Figure 10. Since the design cannot allow large overhangs, all lattice cells need to have at least one beam growing away from the faceplate. This ensures that every cell is supported.

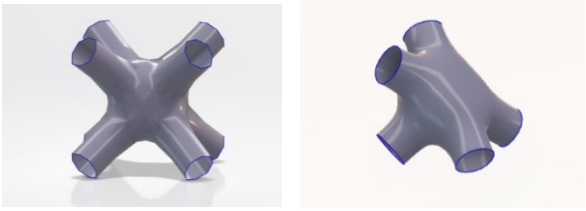

a) b)

Figure 10: Lattice cells, a) 8 beams with p=0.8, b) 7 beams with p=0.6

In order to produce a smooth transition from the lattice to the faceplate, the layer that is closest to the faceplate is slightly modified. The main dimensions and the generation steps are identical but the beams that connect to the faceplate are replaced by a cone-like shape that grows evenly and gradually until it fills the entire faceplate. The elementary cell of this layer can be seen in Figure 11. Just like the lattice cells in the other layers, these cells closer to the faceplate do not necessarily need to have all 4 beams. The number of beams depends on the number of cells from a different layer that connect to the cell. In some cases a cell can have only one beam. On the other hand the cone-like shape is always present and equal for all cells.

Figure 11: elementary cell closest to the faceplate

Once all the cells are defined they can be put together to form the entire lattice structure. The last operation is the removal of the injector volume that was mentioned above. This boolean operation needs to ensure that inner volume of the injectors is not obstructed by the lattice but at the same time it needs to ensure that the lattice is connecting to the injector walls.

In Figure 12, we see two examples of the final lattice structure on real test pieces. The front view on picture Figure 12.a) shows how all the cells emanate from the injectors walls and grow smoothly until the entire faceplate is covered. It also shows that there are many different variations of the cells depending on the number of beams. In Figure 12.b) we see that not all cells that are close to the faceplate have all the beams. Cells that only have one or two connecting members can sometimes look like gaps in the lattice but they still cover and support the faceplate.

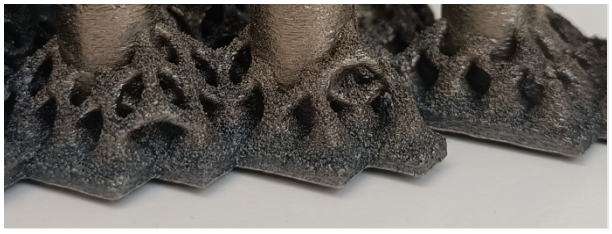

a)

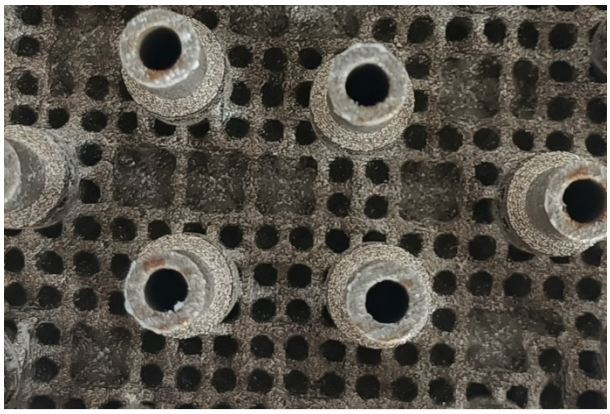

b)

Figure 12: examples of the lattice on test pieces. a) front view, b) top view

2.3. CFD analysis

The objective of the CFD simulations is to get a first estimation of the heat transfer coefficient on the lattice that can serve as a boundary condition for a FEM simulation of the injector head. This is an important first step since it is the first time the injector head is tested and the thermal loads of these specific injectors are unknown in a full scale configuration with nominal load points. Performing a CFD simulation of the entire dome with the lattice structure is quite complex, due to the intricate structure of the lattice. Additionally, the lattice structure is generated with many polyhedral surfaces to create a very smooth geometrical model, but this poses some additional constraints on the handling of such files for numerical analysis. For these reasons the problem is simplified to include a few elements of the lattice, similar to what was done in [10,11] and the geometric representation is also simplified by only including the main features of the elements before the smoothing step. In [11] it is shown that the heat transfer of a lattice cell is affected by the flow from a previous lattice. With this in mind the fluid domain for this simulation includes an inlet and an outlet development region with a length of 2L and in the middle there is a 2x2 cube of lattice elements (see Figure 13).

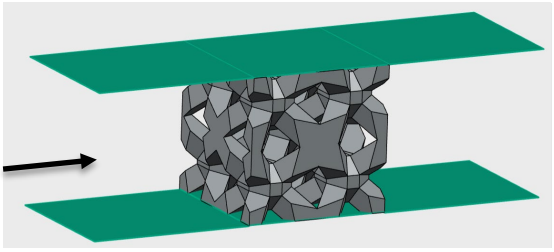

Figure 13: Computational domain for CFD

It is evident that this represents a very large simplification of the real conditions. The flow inside the propellant dome is much more heterogeneous than the flow conditions in this fluid domain so we cannot expect these simulations to provide an exact value of the heat transfer coefficient.

This also makes the definition of the boundary conditions quite complex leading to relevant simplifications. The Table 1 contains a list of boundary conditions used in the simulation.

	Velocity	Temperature	Pressure
Inlet	Fixed value	Zero gradient	Zero gradient
Outlet	Zero gradient	Zero gradient	Fixed Value
Channel walls	Symmetry	Symmetry	Symmetry
Lattice	No slip	Fixed value	Zero gradient

Table 1: boundary conditions of the CFD

In order to get a value for the inlet velocity, a simulation of the propellant dome without the lattice was performed. From this simulation it is possible to extract the velocity field in the region of the lattice. The average value of the velocity of this region defines the reference velocity, V_{ref}. Due to the fact that the introduction of the lattice causes an additional obstruction to the flow which will likely have a negative impact on the flow in this region, two other velocities were considered. These were 15% and 60% of the reference velocity. For the fixed wall temperature three values were considered. These are 35%, 55% and 73% of the temperature limit of the material. Three temperatures were tested to make sure that the heat transfer coefficient will not change depending on this arbitrary wall temperature. The outlet pressure was set at the propellant dome pressure. The turbulent model used is the SST k-omega model.

The mesh is composed by 868 585 polyhedral cells. All mesh quality parameters are within the OpenFOAM standards. The maximum mesh non-orthogonality is 70 and the average is 26.

2.4. Injector plate lattice face plate thermo-mechanical analysis

A steady state Finite Element Method thermo-mechanical analysis has been performed with the commercial ANSYS 23R2 software. A steady state thermal analysis is performed and implemented, as an input, into the steady state structural analyses of the Huracan Inocnel718 heat treated injector head. The aim of the analysis is, on one hand, to assess the use of innovative and pioneer lattice structure[1] design. On the other hand, is to explore the stressed areas of the structure from a thermal and mechanical perspective in order to improve the injector head structural design.

The analysis is performed considering 1/6 3D slice of the Huracan real scale injector head. Symmetrical thermal and mechanical boundary conditions are applied to the sliced walls with respect to the injector head circumferential direction, assuming the axial direction according the engine axis.

Material properties refer to the internal heat treated Inconel718 material characterization activity performed at The Exploration Company in cooperation with Politecnico di Torino DIMEAS laboratory. The model consider same material properties for the injector head, the plate and the lattice structure. Assumption of isotropic thermal properties, as well as mechanical, is done. A bilinear hardening model is used to take into account plasticity at different temperatures.

The analysed hardware has been discretized with a total of 317523 3D tetrahedral elements, leading to 1556279 nodes. For computational reasons, the mesh size tends to be comparable with the lattice structure simplified beams. Since the lattice structure algorithm can only provide a .stl file,

the beams are simplified in order to avoid mesh dependency on the .stl file surface mesh size. A simplification hypothesis has been done, assuming squared beams (Figure 14), instead of the real cylindrical shape. An equivalent cross section area is employed, thus the computed stresses and material lattice limit can be compared.

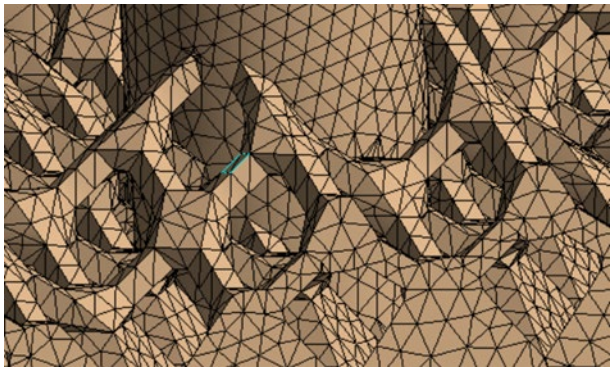

Figure 14: Huracan lattice structure injector head tetrahedral mesh

Mechanical boundary conditions consist in the main combustion chamber nominal operative pressure imposed on the hot gas side of the face plate, together with the oxidiser and fuel operative pressures in the domes of the injector head. It is of primary importance to model the interaction between the injector head flange and the main combustion chamber, thus the face plate mechanical behaviour is as accurate and realistic as possible. Because of the aforementioned reason, the injector head interface with the main combustion chamber has been replicated by means of mechanical constraints. These conditions are imposed on a way to be able to replicate and take into account the main combustion chamber behaviour.

Thermal boundary conditions have been implemented by a combination of literature studies and experimental temperature restitution internal activity from the water-cooled test camping performed at P8 DLR test facility in Lampoldshausen. Oxidizer dome and manifold assume a constant heat exchange coefficient, according to common flat surface heat exchange problems [12], and the bulk oxygen temperature acquired from the test data. Fuel dome and manifold assume a constat heat exchange coefficient and the fuel bulk temperature with the same logic of the oxidiser dome and manifold. The heat exchange on the lattice structure mesh has been modelled using heat exchange computed by the CFD analysis, presented in the frame of this work, and the expected fuel bulk temperature. A constant calibrated heat exchange coefficient has been used for the face plate thermal model. The calibration is performed by using intrusive thermocouples into the face plate and the gradient method. The boundary condition refers to the most sever hot fire test performed during the water-cooled test campaign.

[1] Patent submitted

2.5. Additive manufacturing process of lattice structure specimens and testing set up

Additive manufacturing specimen of the lattice structure have been produced in order to test the mechanical limits of the pioneering lattice structure introduced into the face plate. The aim of testing is not to extrapolate the mechanical material properties of the lattice structure beams, but rather to evaluate the limits, in terms of ultimate strength, of the interface between the lattice structure and the bulk material links by comparing the uniaxial test with the computed Von-Mises stresses at the interface. Lattice structures tend to fail at the interface between beams and the geometry [13]. This is mainly due to stress intensification reasons and because of the additive manufacturing machine laser switching from parameters used on the bulk material and the lattice beams [14].

The specimens have been additive manufactured with a TRUMPF TruPrint 3000 system and a standard precipitation hardening vacuum heat treatment has been performed.

The specimen geometry has been created by using the same lattice structure geometry and lattice to face plate connection strategy of the Huracan injector head and presented in Figure 15. Specimens have been printed in vertical direction because of the analogy with the orientation of the lattice structure of the real injector head, thus the specimen axis is parallel to the building direction of the additive manufacturing process.

The geometry consist of a squared gauge length area made out of lattice structure. Beams are linked to a top and a bottom squared plate with the same algorithm used for the injector head.

The room temperature tensile set-up consist of a INSTRON 100kN hydraulic testing machine. A displacement control of 1mm/min is used and an extensometer is attached to the bulk areas of the specimen. A total of 3 tensile samples have been tested.

Room temperature compression test set-up uses the same hydraulic machine equipped with compression parallel plate grips. Displacement control is set to be 1mm/min and no extensometer have been employed. Displacement is tracked with the main machine piston movement encoder system.

Finally, a 300kV Fraunhofer IKTS 5 micron resolution CT has been used to characterise the surface of the specimens and compute the beam diameter deflection from nominal dimensions. The last has a primary importance to compute the uniaxial ultimate strength at the fracture spot.

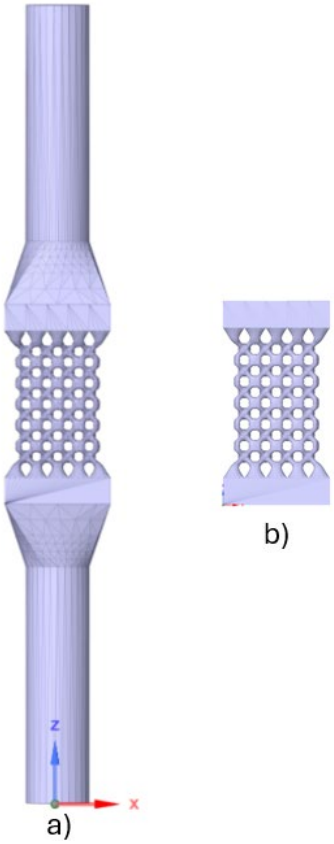

Figure 15: Huracan lattice structure injector head traction a) and compression b) specimens.

3. RESULTS

3.1. CFD analysis

The first step of the analysis is to determine whether the mesh resolution near the one is fine enough to resolve the boundary layer. This is especially important in heat transfer problems. For this purpose it is common to use the y^+ values. In general it is said that a y^+ value close to unity is necessary to resolve the viscous sublayer [15]. In Figure 17, we see that the y^+ value ranges from 1 to 9, with the higher values located at the edges of the lattice where regions of higher velocity exist. The average y^+ value is 3 and this is considered fine enough for this simulation.

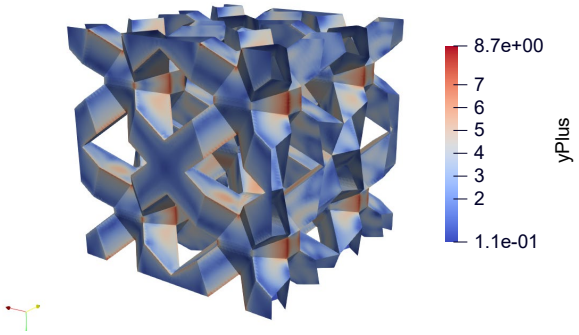

Figure 16: y^+ value of the lattice simulation

In order to visualize the flow pattern, velocity contours are plotted Figure 18 in the midplane of the channel aligned with the flow direction and in a normal plane that is located between the lattice elements. Since the lattice structure is a body centred cubic (BCC) lattice, its interstices align and create regions of high velocity which in this case can be up to 5 five times higher than inlet velocity. Additionally, BCC lattice creates a checkboard pattern, meaning that there are alternating regions of low and high velocity. The low velocity regions are caused by recirculation zones. These regions are responsible for an increase in turbulent kinetic energy which increases mixing and convection.

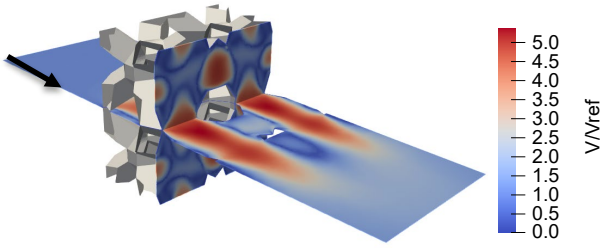

Figure 17: velocity contours in the two midplanes of the channel

Finally using the inlet temperature and the fixed wall temperature together with the computed heat flux from the simulation it is possible to extract the estimation for the heat transfer coefficient. The heat transfer coefficient of the case using V_{ref} as the inlet velocity and the $0.55T_{limit}$ as the wall temperature was used to normalize the values.

The results can be seen in Table 2. Naturally, as we decrease the inlet velocity the heat transfer coefficient decreases as we would expect. Additionally, the different wall temperatures do not have a significant impact on the heat transfer coefficient. The influence of subsequent lattice elements was also confirmed by these simulations. The second layer of lattice elements showed a decrease of 5% of the heat transfer coefficient for the simulations with V_{ref} as the inlet velocity. For the lower velocities this discrepancy was as high as 9%, showing that in this case there is a significant change of heat transfer coefficient.

V/V_{ref}	0.15	0.6	1
h/h_{ref}	0.32	0.65	1

T_{wall}/T_{limit}	0.35	0.55	0.73
h/h_{ref}	0.98	1	1.05

Table 2: heat transfer coefficients. Top) fixed wall temperature at $0.55T_{limit}$. Bottom) fixed velocity at V_{ref}

3.2. Lattice mechanical characterization

The tensile test results, as illustrated in Figure 19 and normalized relative to the maximum value of the reference parameter, offer valuable insights into the

mechanical behaviour of the material. The force-displacement curve, when normalized, reveals a mechanical response akin to that of typical lattice structures. Notably, the lattice structure exhibits an initial phase of linear elasticity, followed by yielding within the plastic domain. This plastic deformation phase is characterized by a quasi-linear hardening behaviour. The point of fracture closely aligns with the ultimate strength of the structure, indicating a critical failure threshold. Moreover, the repeatability of the force-displacement curve demonstrates consistency in terms of elongation to fracture across multiple tests. However, it is noteworthy that slight deviations in elasticity behaviour are observed among tested specimens.

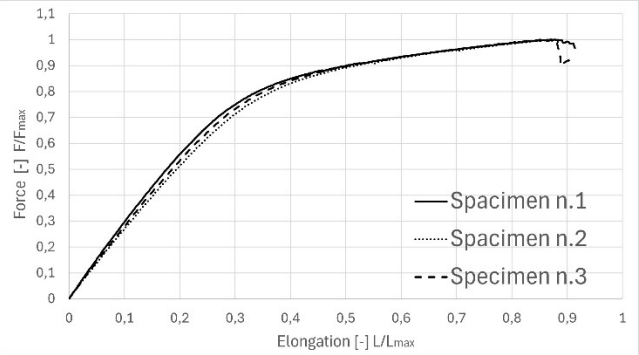

Figure 18: Normalised force-displacement curve of room temperature tensile tests

Analysing the compression test results, normalized relative to the maximum value of the reference parameter depicted in Figure 20, a comparison with the behaviour observed in tensile specimens is warranted. Overall, the mechanical response exhibits similarities to that observed in tensile tests. However, notable discrepancies arise in the elongation to fracture across specimens, particularly evident when comparing specimen n.1 to n.3. Furthermore, disparities are observed in the ultimate strength and stress at the fracture point among tested specimens. These variations may be attributed to inherent material heterogeneity, manufacturing inconsistencies, or other extraneous factors influencing the mechanical response.

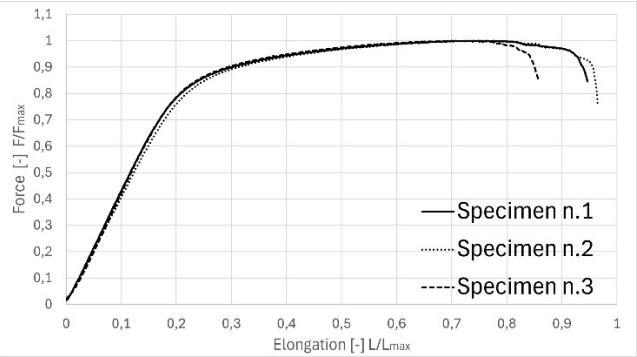

Figure 19: Normalised force-displacement curve of room temperature compression tests

Observations from both tensile and compressive tests reveal that fracture initiation predominantly occurs at the interface. In the case of tensile tests, a distinct horizontal fracture plane is evident, perpendicular to the vertical loading direction of the specimen. However, a closer examination under the microscope reveals localized regions where beams exhibit a 45° fracture orientation relative to the loading direction (refer to Figure 21). Notably, fracture consistently occurs in the top region relative to the vertical printing direction for all tensile specimens, despite the symmetric geometry of the specimen, wherein the top and bottom areas are theoretically identical.

Conversely, compression tests exhibit a 45° fracture plane with the fracture starting point consistently located at the top right corner relative to the printing direction (refer to Figure 22). It is noteworthy that this starting fracture area aligns with that observed in tensile specimens. This consistent observation across compression bench specimens further reinforces the significance of the identified weak point in the structure's top area. Despite the theoretical symmetry of the specimen geometry, practical observations underscore the asymmetrical distribution of stress and strain, emphasizing the critical role of localized structural characteristics in governing fracture initiation and propagation.

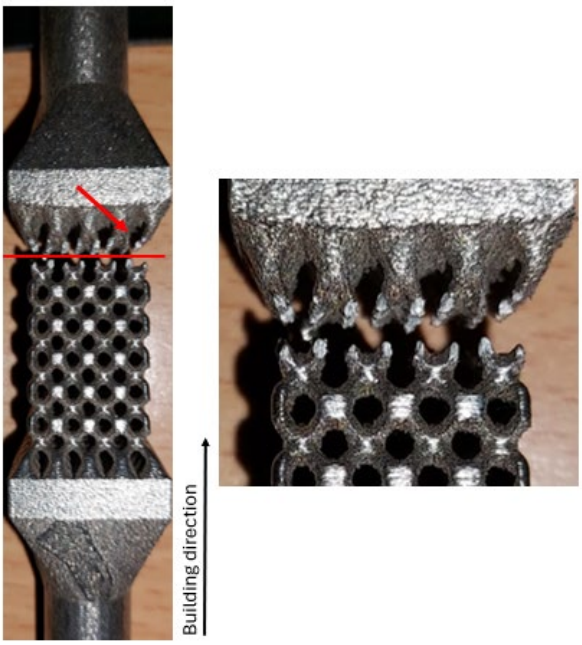

Figure 21: Room temperature tensile tests

Through a comprehensive analysis of the CT scan results delineated in Figure 23, with a focused examination on both the upper and lower beams, a dissimilarity in surface roughness becomes evident. The presence of surface irregularities on the upper beams provides a possible justification for the fracture localization observed in the tensile specimens and marks the initiation site of fracture in compression tests. It is imperative to note that

surfaces characterized by pronounced roughness exhibit a propensity to defects, consequently leading to optimized for printing lattice structure beams to those tailored for fabricating bulk conical basement supports.

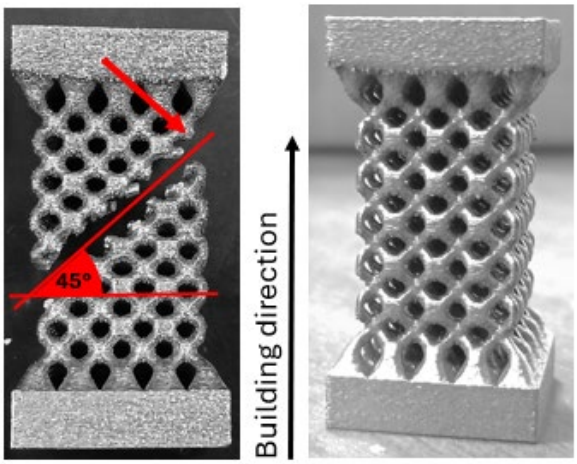

Figure 20: Room temperature compression tests before (right) and after (left) fracture

This nuanced insight underscores the intricate interplay between process parameters and structural integrity, elucidating the multifaceted nature of additive manufacturing processes in engineering applications.

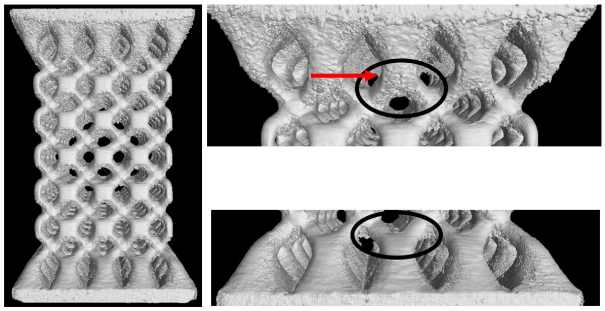

Figure 21: CT scan of tensile tests specimen and comparison between surface quality of the top and the bottom link cone areas

3.3. Thermo-mechanical analysis

The incorporation of a lattice structure into the design of the face plate offers two primary advantages. Firstly, computational fluid dynamics (CFD) analysis reveals a notable increase in heat exchange accompanied by an expansion in the total heat exchange area. This enhancement in heat transfer capabilities is instrumental in optimizing thermal management within the system. Additionally, the thermomechanical behaviour benefits from these improvements, as evidenced by lower temperatures and stresses compared to a conventional flat injector face plate structure.

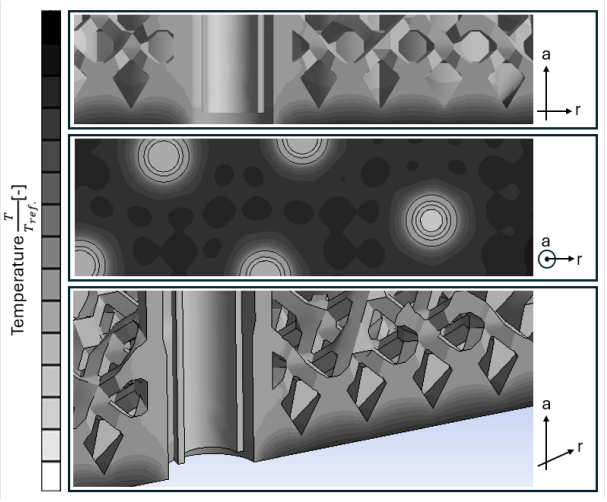

Figure 22: Normalised temperature distribution in the injector head lattice structure

The thermal map of the injector head lattice structure, presented in Figure 24 radial images, illustrates the significant impact of the lattice implementation. A comprehensive analysis reveals that the majority of the beams exhibit temperatures comparable to that of the bulk fuel temperature. This observation underscores the effective heat dissipation capabilities facilitated by the lattice structure. Conversely, the most pronounced temperature disparities are observed in the conical supports, which intersect to form the face plate. The convergence of these conical supports creates localized regions of elevated temperature, attributable to the concentrated thermal energy exchange occurring within these structural elements.

Figure 24 axial image presents the temperature distribution across the face plate, replicating the conical links between the lattice structure and the face plate. A discernible pattern emerges, with the highest temperatures cantered relative to the conical base. This phenomenon arises due to the concentrated thickness of the face plate within the central region of the cones. Conversely, the lowest temperatures are observed in the circular areas proximal to the injectors. This disparity can be attributed to the inherently lower temperatures of the fuel and oxidizer, coupled with the heightened velocity facilitating enhanced heat exchange in these regions.

Upon analysing the temperature distribution within a single conical support of the lattice structure, it becomes evident that the highest temperatures are concentrated at the bottom (refer to Figure 25) and in the middle sections (refer to Figure 26) of the cone structures. This spatial distribution of temperature highlights the localized heat accumulation within these regions.

Furthermore, examination of the vertical temperature profile (Figure 25) reveals an asymptotic behaviour in proximity to the first beam interception of the lattice structure. This observation suggests a gradual decrease in temperature with increasing distance from the intersection point,

indicative of the dissipation of thermal energy along the vertical axis of the conical support.

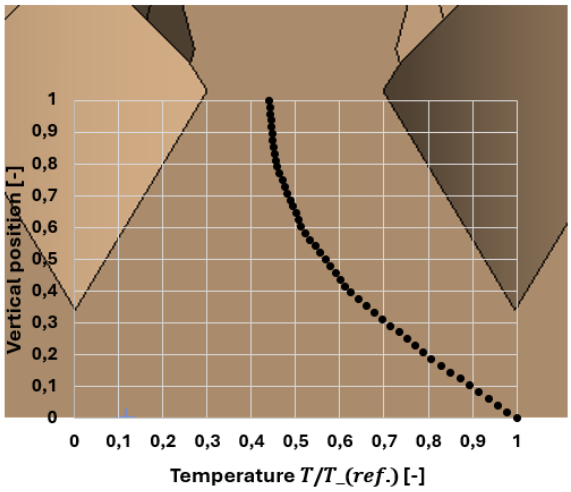

Figure 23: Normalised temperature vs vertical position of single lattice structure cone support

Considering the radial distribution of temperature (Figure 26) within the conical support, a bell-shaped profile is evident. This distribution pattern, characteristic of bell distributions, indicates that temperatures are highest at the centre of the radial cross-section and gradually decrease towards the periphery. The bell distribution of temperature suggests that heat is distributed symmetrically around the central axis of the conical support, with the majority of thermal energy concentrated near the centre.

The equivalent Von Mises stresses depicted in Figure 27 reveal that the highest stress concentrations occur around the injector elements. This observation can be attributed to the pronounced thermal gradients present in these regions, as discussed earlier. The thermal gradients induce differential expansion and contraction within the material, leading to localized stress concentrations

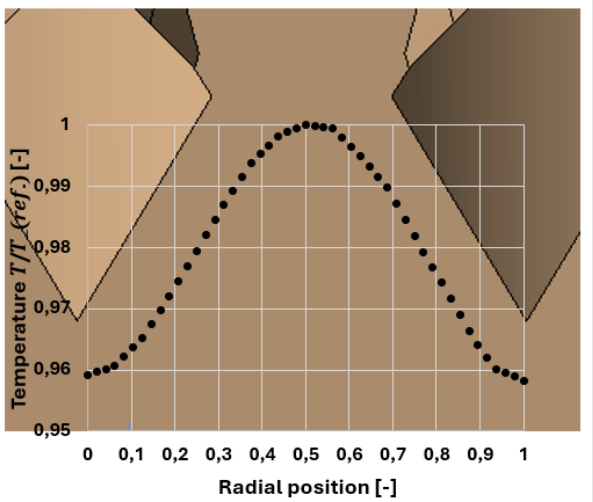

Figure 24: Normalised temperature at the bottom area of a single element conical support vs radial position (with respect to the injector head main symmetry axes)

Moreover, owing to the elevated temperatures experienced, the face plate emerges as a focal point for stress concentration, exhibiting consistently high stress levels. Given the significance of these stress concentrations, it is imperative to compare the Von Mises stresses in these areas with the material properties of bulk specimens. This comparative analysis is essential for computing safety factors and assessing the structural integrity of the hardware under operational conditions.

Directing attention to the lattice structure, it becomes evident that the beams experience higher stress levels (indicated by red arrows in Figure 27) compared to the majority of the conical support areas and compared the points where the beams intersect. This observation underscores the critical role played by the beams in bearing mechanical loads and transmitting forces from the face plate to the lattice mesh itself and the injectors columns. This effect is a clear benefit for the face plate, contributing to reducing stresses in the highest temperature area of the injector head and raising it to the area where temperature is lower.

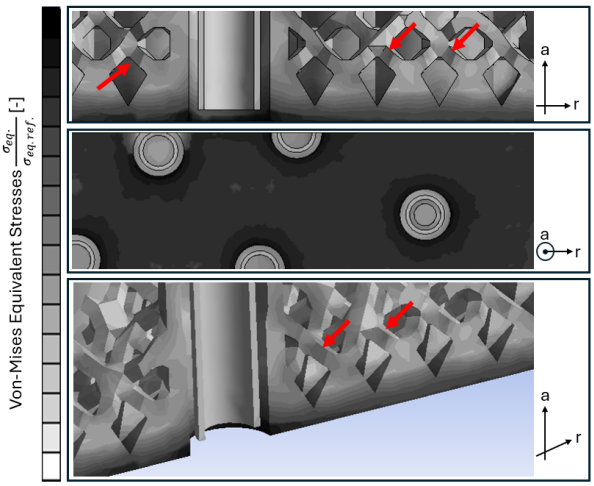

Figure 25: Normalised Equivalent Von-Mises stresses distribution in the injector head lattice structure

By distributing stress more evenly throughout the lattice structure, particularly by relieving stress concentrations in the highest temperature regions, the lattice design effectively reduces the risk of structural failure due to thermal stresses. This is crucial for maintaining the integrity and longevity of the injector head under demanding operating conditions. Furthermore, by equalizing stress levels across the face plate, the lattice structure enhances its overall structural resilience and performance. This ensures that the face plate can withstand thermal and mechanical loads without succumbing to premature failure, thus improving the reliability and efficiency of the injector head assembly.

Since beams play a relevant role and are high loaded it is of primary importance to deeply study the mechanical behaviour at the interface with the conical supports. Because of these reasons lattice structure

specimens have been tested and results compared with Von-Mises equivalent stresses.

Equivalent Von-Mises stresses in the conical supports show a similar trend to the temperature distribution earlier presented. Stresses are concentrated to the bottom of the cones, thus the face plate and converge to the lowest value of 4% from the 30% of the hight on. For the radial distribution, the bell-shaped profile is present but not as symmetric as the temperature profile. This is attributed to the mesh element size, the non-uniform loading due to the not perfect symmetricity of the geometry.

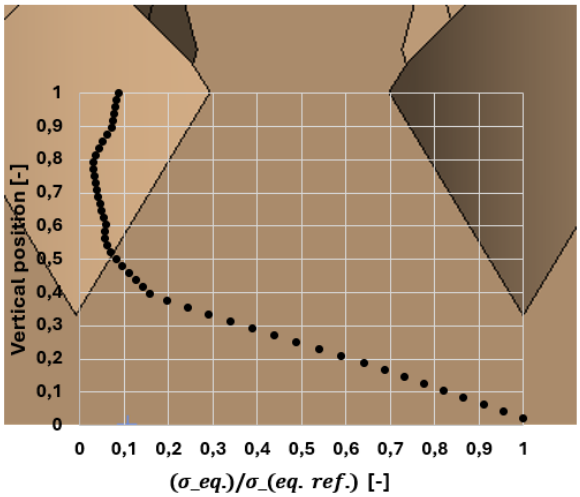

Figure 26: Normalised Equivalent Von-Mises stresses vs vertical position of single lattice structure cone support

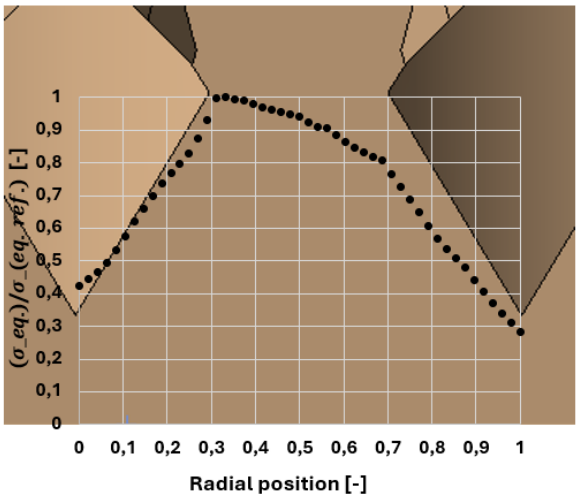

Figure 27: Normalised Equivalent Von-Mises stresses at the bottom area of the conical support vs radial position (with respect to the injector head main symmetry axes)

3.4. TCA1 water cooled test campaign

The results from the test campaign show a strong dependency of the faceplate temperatures with the chamber pressure. In Figure , we see one hot fire test from the campaign, where the thrust chamber was throttled from 50% to 100%. In the graph it is clear that for lower chamber pressures the temperatures decrease. The reason for this is unknown but it is likely due to the changes in the injection momentum. When the pressure is higher, the propellants are injected with higher mass flow rates and therefore higher velocities. This means that the flame might be anchored further away from the faceplate which would lower the heat flux.

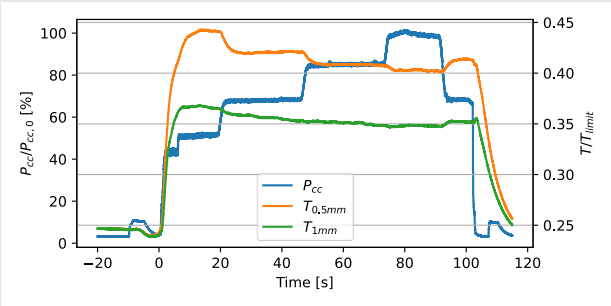

Figure 28: Faceplate temperature ($T_{0.5mm,1mm}$) dependency on the chamber pressure (p_{cc})

In Figure 31 and Figure 32 we see the faceplate temperatures for the entire test envelope. The temperatures are normalized by the temperature limit of the material, which is the temperature when the mechanical properties start to decrease very rapidly. Besides the pressure dependency that we saw above we can also see a weak dependency on the mixture ratio, where higher mixture ratios cause higher temperatures. The hottest temperature that was measured at the 0.5mm depth was $0.44T_{limit}$, while at the 1mm depth was $0.37T_{limit}$. These temperatures were measured at 33% chamber pressure and nominal mixture ratio.

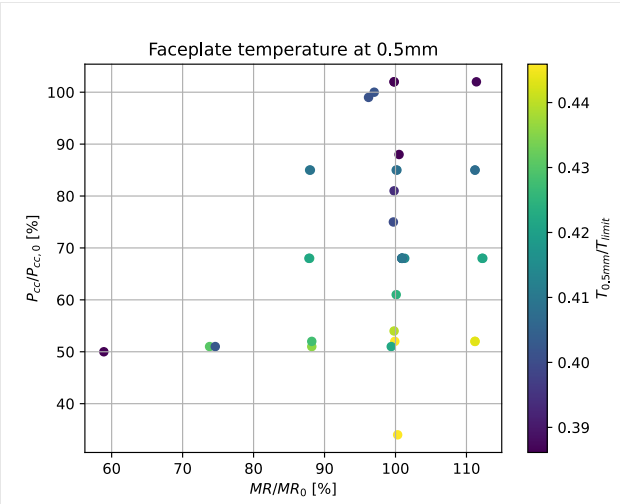

Figure 29: Normalized temperature at 0.5mm from the faceplate over mixture ratio and chamber pressure

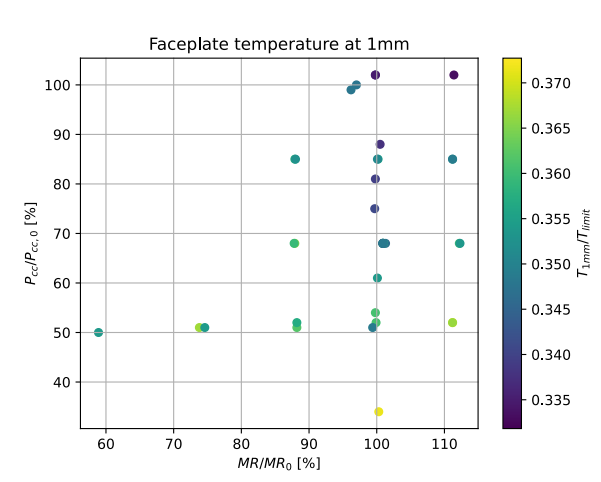

Figure 30: Normalized temperature at 1mm from the faceplate over mixture ratio and chamber pressure

The fact that we have two thermocouples at different depths allows us to estimate the heat flux by the gradient method. The gradient method is a very simple calculation of the heat flux that considers 1D heat conduction. In a faceplate the heat conduction is not 1D so the calculation is not exact. The calculation also assumes a constant thermal conductivity, κ, but due to the strong temperature variations this might not always be true. In our case the temperature difference between the 0.5mm and 1mm depth is small so this assumption is valid. The calculation of the heat flux using the gradient method is

$$q = \frac{\kappa}{\delta}(T_{0.5mm} - T_{1mm}) \qquad \text{Eq.1}$$

where q is the heat flux and δ is the distance between thermocouples, in this case 0.5mm. The results of this computation can be seen in Figure 32 and the same dependencies on the pressure and mixture ratio can be seen.

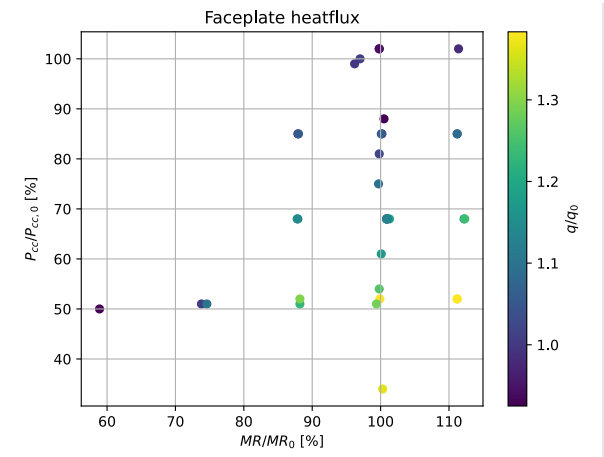

Figure 31: Faceplate heat flux computed with the gradient method

Finally, using these values we can estimate the heat transfer coefficients both on the hot side and cold side. In order to do this it is necessary to have two reference temperatures, one for the cold side gas temperature and one for the hot gas side temperature. For the cold side gas temperature, the reference temperature was the methane temperature measured at the propellant dome. For the hot side gas temperature, the Chemical Equilibrium and Applications (CEA) [11] was used to compute the adiabatic combustion temperature. With these reference temperatures the heat transfer coefficient can be computed with

$$h = \frac{q}{(T_1 - T_2)} \qquad \text{Eq.2}$$

where h is the heat transfer coefficient and T_1 and T_2 are the wall temperatures and the gas temperatures depending on the direction of the heat flux. Interestingly, using this approach the heat transfer coefficient that is obtained is three times higher than the one obtained in the CFD simulation. The main reasons for these discrepancies are the strong simplifications and conservative boundary conditions use in the CFD and the heat transfer enhancement caused by high surface roughness of 3D printed parts [10].

4. CONCLUSION

In the present work an innovative cooling strategy for LOX-Methane liquid rocket engine injector head has been presented. Computational Fluid Dynamics analysis has been performed ac used as boundary condition for the thermo-structural analysis. A calibrated heat flux has been used to simulate the main combustion chamber hot gasses during the TCA1 water cooled test campaign performed at P8 DLR Lampoldshausen test facility. Results shows thermal and mechanical benefits of using the new face plate lattice structure design.

In particular, the lattice structure design is able to increase the heat exchange coefficient on the injector face plate that faces the liquid dome. The lattice structure, because of this geometry, is able to increase turbulence and therefore the heat exchange, driving out heat from the face plate and therefore lowering its temperature.

Increase the mechanical resistance of the face plate without increasing the thickness is another remarkable effect. The face plate can benefit of the lattice structure to increase the stiffness and therefore reduce the face plate thickness. This allows a weight reduction compared to conventional face plate, which increases the face plate stiffness by increasing the plate thickness, leading to higher temperatures.

Finally, the new proposed design solution is able to avoid a multi-component injector head. Prior realizations of the component often use a multi-step assembly approach with conventional manufacturing

processes. In many cases, the single injector elements are manufactured and then assembled (through e.g. threading or welding) to form the final injector head component. This could be hundreds of single manuals working steps until all injectors are integrated.

5. REFERENCES

1. Additive Manufacturing of Liquid Rocket Engine Combustion Devices: A Summary of Process Developments and Hot-Fire Testing Results - Gradl, Paul, Greene, Sandy & Protz, Christopher & al. (2018).

2. Robust Metal Additive Manufacturing Process Selection and Development for Aerospace Components - Gradl, Paul and Tinker, Darren C. and Park, Alison and Mireles, Omar R. and Garcia, Marissa and Wilkerson, Ryan and Mckinney, Christopher (2022). *Journal of Materials Engineering and Performance*

3. Analysis of Heat Transfer Characteristics of a Heat Exchanger Based on a Lattice Filling - Lai, X.; Wang, C.; Peng, D.; Yang, H.; Wei, Z. (2021). *Coatings*

4. Application of Ceramic Lattice Structures to Design Compact, High Temperature Heat Exchangers: Material and Architecture Selection - Pelanconi, M.; Zavattoni, S.; Cornolti, L.; Puragliesi, R.; Arrivabeni, E.; Ferrari, L.; Gianella, S.; Barbato, M.; Ortona, A. (2021). *Materials*

5. Damping device to reduce the risk of injection-coupled combustion instabilities in liquid propellant rocket engines - Armbruster, Wolfgang and Hardi, Justin S. and Miene, Yannik and Suslov, Dmitry and Oschwald, Michael (2020). *Acta Astronautica*

6. Advanced rocket engine – Oskar J. Haidn (2015)

7. Propellant Atomization for Porous Injectors - Deeken, J. C. and Suslov, D. I. and Oschwald, M. and Schlechtriem, S. and Haidn, O. J. (2019). *Journal of Propulsion and Power*

8. Porous Medium Modeling for Liquid Rocket Injector Flows - Sozer, Emre and Law, Ryan and Carroll, Bruce and Thakur, Siddharth and Shyy, Wei and Tucker, Kevin (2006). *American Institute of Aeronautics and Astronautics*

9. NUMERICAL MODELING OF TRANSPIRATION COOLED ROCKET - Tully, Landon Rothwell

10. Stimpson, Curtis; Snyder, Jacob;Thole, Karen; Mongillo, Dominic - Roughness Effects on Flow and Heat Transfer for Additively Manufactured Channels (2015). *Journal of Turbomachinery*

11. Computer Program for Calculation of Complex Chemical Equilibrium Compositions and Applications - S. Gordon; B. J. McBride (1996). *NASA Reference Publication 1311*

12. Incropea's principes of heat and mass transfer – Incropea et al. (2017).*Book*

13. Elastic and failure characteristics of additive manufactured thin wall lattice structures with defects - Wu, Yan and Yang, Li (2021). *Thin-Walled Structures*

14. Fatigue life of additively manufactured Ti6Al4V scaffolds under tension-tension, tension-compression and compression-compression fatigue load - Lietaert, Karel and Cutolo, Antonio and Boey, Dries and Van Hooreweder, Brecht (2018). *Scientific Reports*

15. Turbulence Modeling for CFD (Third Edition) (Hardcover) - Wilcox, David. (2006).

6. Acknowledgments

Special thanks goes to the team of the P8 test bench of DLR, as Alex Grebe and Markus Dengler in realizing the experiments presented in this paper.

Additionally, special thanks to Toolcraft and HycAero for manufacturing the components of the thrust chamber.

Finally, special thanks to CNES for sharing their test days at the P8 test bench and ESA and BPI for funding of the development of the Huracan engine.